Electronic and Geometric Effects of Phosphatriazaadamantane Ligands on the Catalytic Activity of an [FeFe] Hydrogenase Inspired Complex

Aaron K. Vannucci, Shihua Wang, Gary S. Nichol, Dennis L. Lichtenberger, Dennis H. Evans*[†], and Richard S. Glass**

Contribution from the Department of Chemistry and Biochemistry, The University of Arizona, Tucson, AZ 85721-0041

AUTHOR EMAIL ADDRESS: rglass@email.arizona.edu, evansd@purdue.edu dlichten@email.arizona.edu

ABSTRACT: The [FeFe] hydrogenase enzyme active site inspired complexes [$Fe_2(\mu\text{-}C_6H_4S_2)(CO)_5PTA$] (**1PTA**) and [$Fe_2(\mu\text{-}C_6H_4S_2)(CO)_4PTA_2$] (**1PTA$_2$**) (PTA = 1,3,5-triaza-7-phosphaadamantane) were synthesized and characterized. The ability of **1PTA** and **1PTA$_2$** to catalytically produce molecular hydrogen in solution from the weak acid acetic acid was examined electrochemically and compared to previous studies on the all carbonyl containing analogue [$Fe_2(\mu\text{-}C_6H_4S_2)(CO)_6$] (**1**). Computational methods and cyclic voltammograms indicated that the substitution of CO ligands by PTA in **1** resulted

---

[†] Present address: Department of Chemistry, Purdue University, West Lafayette, IN

in markedly different reduction chemistry. Both **1PTA** and **1PTA$_2$** catalytically produce molecular hydrogen from acetic acid, however, the mechanism by which **1** and **1PTA** and **1PTA$_2$** catalyze hydrogen differ in the initial reductive processes.

Introduction

[FeFe] hydrogenase enzymes are well known to catalyze the production of molecular hydrogen from protons and electrons with extremely high efficiency.[1] The active sites of the [FeFe] hydrogenases contain an 2Fe2S core that has inspired extensive work on developing simple and robust structural analogues that may mimic the catalytic activity of the enzymes. The study of hydrogenase inspired catalysts has become so wide spread that many recent review articles on the topic have been published.[2-6]

<AS and 1.tif here>

One such hydrogenase inspired catalyst is 1,2-benzenedithiolato diiron hexacarbonyl (**1**), which has been shown to catalytically produce molecular hydrogen from acetic acid in an acetonitrile solution.[7] The benzenedithiolate (bdt) ligand helps modulate the redox reactions of the catalyst by lowering the potential difference between successive reduction states. Delocalization of the electron density into the bdt moiety upon reduction of the diiron core results in large geometric changes in the anion. These geometric changes, shown in Scheme 1, allow for potential inversion, the insertion of a second electron at a lower potential than the initial reduction, and the formation of a dianion species ($\mathbf{1}^{2-}$). As can be seen in Scheme 1, one $Fe(CO)_3$ moiety rotates upon reduction of the neutral molecule to the anion, so that a carbonyl ligand can bridge between the two Fe atoms. Formation of the bridging CO is accompanied by cleavage of an Fe-S bond, and this large geometric change is what allows for the formation of a dianion with potential inversion. It also contributes to the stability of the dianion and the reversibility of the two-electron reduction process. The bdt ligand disfavors the dimerization or CO loss degradation pathways with reduction that have been observed with reduction of other dithiolate diiron complexes.[5,8-11] The $Fe(CO)_3$ rotation, followed by Fe-S bond cleavage and a bridging of a CO ligand around the diiron center also opens up a favorable site for protonation, and the dianion is sufficiently basic to be protonated by weak acids such as acetic acid. The protonated species is then reduced at a more negative potential, which generates a reactive hydride dianion. The hydride dianion then reacts with another molecule of acetic acid and efficiently produces molecular hydrogen.

While the bdt moiety offers favorable properties for catalysis, bdt also decreases the reactivity of the 2Fe2S core. The delocalization of the electron density into the conjugated π-system of the bdt moiety lowers the basicity of the diiron core. Since protonation occurs at the diiron core and protonation is the rate-determining step of the catalytic mechanism,[7] lowering the basicity decreases the extent of protonation and decreases the catalytic activity. Developing a catalyst with increased electronic density at the iron center in conjunction with the favorable properties of benzene dithiolate ligation, therefore, could lead to improved catalysis.

While the hydrogenase enzyme utilizes CN^- ligands, phosphorus-containing ligands are more commonly used to alter the electron density of metal-carbonyl complexes.[12-16] For example, $[Fe_2(bdt)(CO)_5(P(OMe)_3]$ has recently been studied[15] as have PNP complexes of other diiron systems.[16] Furthermore, the PMe_3 ligand has even been shown to have similar electronic properties to CN^-,[17] and has been used in electrochemical studies of hydrogenase mimic complexes.[18-20] However, PMe_3 complexes are only soluble in organic solvents, therefore, a more appealing phosphine ligand is 1,3,5-triaza-7-phosphaadamantane (PTA) due to the increased hydrophilicity of PTA over PMe_3.[21-23]

In the present paper, the new catalysts [$Fe_2(\mu\text{-}C_6H_4S_2)(CO)_5PTA$] (**1PTA**) and [$Fe_2(\mu\text{-}C_6H_4S_2)(CO)_4PTA_2$] (**1PTA$_2$**) have been synthesized and studied with electrochemical and computational methods. The catalytic efficiencies of **1PTA** and **1PTA$_2$** are compared to **1** and discussed in terms of the electronic and geometric effects of replacing CO with the PTA ligand. A general catalytic mechanism for the production of molecular hydrogen with the two new catalysts is also proposed.

<PTA structures.tif here>

Experimental

Reagents and instruments

All reactions were performed under N_2 using standard Schlenk line techniques. Purification of the products was performed in air. PTA was used as purchased from Strem Chemical. All solvents used for synthesis were reagent grade and degassed through three freeze-pump-thaw cycles before usage. Complex **1** was synthesized according to previously reported procedures.[24] The ^{1}H, ^{13}C, and ^{31}P NMR spectra were collected in $CDCl_3$ using a Varian Unity-300 with TMS as an internal reference for ^{1}H and ^{13}C and H_3PO_4 as an external reference for the ^{31}P NMR. IR spectra were collected on a Nicolet 380 FT-IR.

Computations

All computations were performed using ADF2006.01d.[25] Computational methods have been described previously.[7] Our comparisons of the OPBE functional, used in this work to calculate the electronic energies of the complexes, to other common functionals in the ADF package have shown it to be among the best at predicting reduction potentials and ionization energies of several iron complexes and the pK_a of the acid included in this study. All electronic structures with unpaired spin were calculated using an unrestricted framework. Only low-spin complexes have been analyzed. The theoretical stretching frequencies for all species were calculated analytically and the lack of imaginary frequencies for the global minimum energy structures showed that the geometries were true minima. Computations on higher energy conformations were inputted with the rotated ligands and allowed to optimize, indicating that those geometries are local minima.

Preparation of 1PTA and 1PTA$_2$

[Fe$_2$(μ-C$_6$H$_4$S$_2$)(CO)$_5$PTA] (1PTA). In a 100 mL round bottom flask 0.211g of **1** (0.5 mmol) was dissolved in 25 mL of THF, then 0.079 g (0.5 mmol) of PTA and 0.038 g (0.5 mmol) of $(CH_3)_3NO$ were dissolved in 15 mL of CH_3OH and cannulated into the flask containing **1**. The reaction mixture was stirred at room temperature for 2 h until there was no remaining starting material as indicated by IR spectroscopy. The solvent was removed in vacuum and the product was purified by column chromatography. The first red band eluted with THF gave the desired **1PTA**. Deep red crystals were obtained from a CH_2Cl_2 solution kept at -20 °C. ^{1}H NMR ($CDCl_3$, 300 MHz, ppm): 7.09 (2H), 6.58 (2H), 4.50 (6H), 4.05 (6H). ^{13}C NMR: 212.1, 209.5, 202.6, 127.9, 126.5, 73.5, 56.4, 56.2. ^{31}P NMR: -16.6. IR (CH_2Cl_2, CO stretching, cm^{-1}): 2052 (s), 1993 (s), 1978 (s), 1939 (w). Anal. Calcd for $C_{17}H_{16}Fe_2O_5S_2PN_3$: C 37.17; H 2.92; N 7.65. Found: C 38.16; H 3.10; N 7.35.

[Fe$_2$(μ-C$_6$H$_4$S$_2$)(CO)$_4$PTA$_2$] (1PTA$_2$). Complex **1** (0.421 g, 1 mmol) was dissolved in 25 mL of THF. To the red-orange solution, 0.312 g (2 mmol) of PTA dissolved in 15 mL CH_3OH was added via cannula. The reaction mixture was stirred at

45 ^{o}C for 22 h. IR spectroscopic analysis showed the absence of starting material and the solvent was removed in a vacuum. The deep red solid was washed three times with 30 mL of hexanes, then dissolved in $CHCl_3$ and dried with anhydrous $MgSO_4$. Crystals were grown from a CH_2Cl_2 solution at -20 ^{o}C. ^{1}H NMR ($CDCl_3$, 300 MHz, ppm): 7.08 (2H), 6.56 (2H), 4.50 (12H), 4.05 (12H). ^{13}C NMR: 209.3, 127.6, 126.1, 73.5, 56.4, 56.3. ^{31}P NMR: -18.3. IR (CH_2Cl_2, CO stretching, cm^{-1}): 2002 (s), 1959 (s), 1936 (m), 1926 (w). Anal. Calcd for $C_{22}H_{28}Fe_2O_4S_2P_2N_6$: C 38.95; H 4.13; N 12.39. Found: C 38.77; H 4.14; N 11.66.

Electrochemistry.

All electrochemical solutions (anhydrous acetonitrile, Aldrich; no additional drying was carried out) were purged with N_2 for twenty minutes before measurements were performed. Each solution contained 0.10 M Bu_4NPF_6 as the supporting electrolyte. All experiments were performed with a model 273 EG&G Princeton Applied Research potentiostat (PAR 273). When acquiring data at scan rates less than 1 V/s, the 5.3 Hz filter on the PAR 273 was used. Above 1 V/s, the 590 Hz filter was used.

The electrochemical cell was water-jacketed, and the temperature was maintained at 25 °C. The volume of the cell used was 25 mL. The working electrode was a 3-mm diameter glassy-carbon electrode (Bioanalytical Systems). The counter electrode was a coil of platinum wire (99.99%). The home-built reference electrode was a silver wire in contact with a solution of 0.10 M Bu_4NPF_6 (98%, Fluka) and 0.010 M $AgNO_3$ (Aldrich) in acetonitrile. The reference electrode was separated from the contents of the cell by means of a porous Vycor frit. When not in use, the reference electrode assembly was kept immersed in 0.10 M Bu_4NPF_6/acetonitrile to prevent drying of the frit.

The working, reference, and counter electrodes were held in the same relative position in the cell throughout all the experiments to ensure that the uncompensated solution resistance remained constant. Prior to all experiments the working electrode was polished on a polishing felt with 1.0-μm alumina paste (Buehler) followed by 0.05-μm aqueous alumina (aqueous, Buehler). The electrode was rinsed with deionized water, ethanol and finally rinsed with acetone, then air dried before usage.

The reference electrode was calibrated with reference to the ferrocenium/ferrocene couple (Fc^+/Fc). This was accomplished by obtaining voltammograms of ferrocene (98%, Aldrich) using the reference electrode and determining the potential of the ferrocene couple with respect to the reference by simulation of the voltammograms. All potentials reported here are referenced to the potential of the ferrocene couple.

X-ray crystallography

Single-crystal X-ray diffraction data for **1PTA** and **1PTA$_2$** were measured on a Bruker Kappa APEXII DUO diffractometer with graphite-monochromated Mo*K*α radiation (λ = 0.71073Å) and a crystal temperature of 150K. Numerical absorption corrections were applied with SADABS;[26] the structures were solved by direct methods and refined by full-matrix least-squares refinement on F^2 using SHELXTL.[27] Molecular graphics were produced with ORTEP-3 for Windows.[28] For both structures hydrogen atoms were initially located from a difference Fourier map; in **1PTA** they were freely refined and in **1PTA$_2$** refined with $U_{iso}(H) = 1.2U_{eq}(C)$ and a C–H distance of 0.98 Å (aryl) and 0.99 Å (methylene). Experimental parameters for both structures are summarized in Table 1; complete sets of geometric parameters are available as Supporting Information.

Results and Discussion

1PTA and 1PTA₂. The synthesis of the PTA-containing complexes occurred through CO replacement on **1** as described in the experimental section. Both **1PTA** and **1PTA$_2$** are air stable. Both complexes are very soluble in $CHCl_3$ and THF, and are soluble in CH_3CN and CH_3OH. The complexes also have a slight solubility in H_2O and neither complex is soluble in hexanes. The shifts in the CO stretching frequencies in the IR spectra for **1PTA** (shifted roughly 70 cm^{-1} lower frequency from **1**) and **1PTA$_2$** (shifted roughly 50 cm^{-1} lower frequency from **1PTA**) are consistent with increased electron density at the 2Fe2S core from phosphine substitutions.

Molecular Structures of 1PTA and 1PTA$_2$

1PTA. Compound **1PTA** crystallized as small translucent red crystal clusters from which a small block was cleaved and found to diffract well, with data measured to a resolution of 0.76 Å using 60 second exposures. The compound crystallizes without solvent in space group $P2_1/c$ with $Z' = 1$ (Figure 1, top), bonding dimensions within the complex are unexceptional.

1PTA$_2$. Large dark red crystals of **1PTA$_2$** were observed to desolvate when removed from the mother liquor and also cracked when flash cooled at 100 K. Data were thus collected on a crystal which was rapidly mounted following removal from the sample vial, and held at 150 K. When all non-hydrogen atoms had been identified final refinement residuals were high, R1 = 0.184 and *w*R2 = 0.50. Application of the twin law 0 0 −1 0 −1 0 −1 0 0, corresponding to a 180° rotation about the [1 0 −1] direction, reduced the residuals to R1 = 0.050 and *w*R2 = 0.137 following five cycles of least-squares refinement; the residuals were reduced further upon inclusion of hydrogen atoms into the structural model and application of a suitable weighting scheme. The final refined twin scale factor is 0.4320(9)

The compound crystallized as a CH_2Cl_2 solvate in space group $P2_1/n$ with $Z' = 2$. One of the CH_2Cl_2 molecules was refined using a two part disorder model with an approximate occupancy ratio of 3:1; the geometry of this molecule was restrained to be similar to that of the ordered molecule. The two unique complexes in the asymmetric unit differ by rotation of an Fe–P bond, placing two otherwise equivalent PTA ligands into different positions. The structure of complex A is shown in Figure 1 (bottom). Within each complex bonding dimensions are unexceptional.

Electrochemical Reduction of 1PTA and 1PTA$_2$

The cyclic voltammograms (CVs) of **1PTA** and **1PTA$_2$** in acetonitrile at varying scan rates are shown in Fig. 2. The CVs, which are normalized on the y-axis to account for variation in the scan rate, give insight into the reversibility of the first cathodic event for both complexes. The top set of voltammograms in Fig. 2 shows that **1PTA** undergoes a reversible reduction with E^o = -1.56 V at all scan rates except for the slowest scan rate, 0.1 V/s, where **1PTA** loses some of the reversibility that was observed at greater scan rates. The loss of reversibility is evident by the smaller anodic peak at -1.56 V and the appearance of a second anodic peak near -1.3 V. The second anodic peak is indicative of a chemical process occurring after reduction to form a new species in solution. One possible chemical reaction that could occur at the slower scan rates is that the reduced species, **1PTA$^-$**, may slowly exchange a CO ligand for a weakly bound solvent molecule,

CH_3CN. This exchange has been previously proposed for phosphine-containing 2Fe2S complexes.[19,23]

The value of $E°$ for **1PTA**, −1.56 V, can be compared to the standard potential for the overall two-electron reduction of **1**, −1.32 V.[6] The 0.24 V negative shift seen upon replacing one CO with PTA is quite comparable to that seen for CO replacement by PTA and other phosphines in complexes similar to those studied here.[2]

The bottom set of voltammograms of Fig. 2 shows that addition of another PTA ligand causes the E^o of **1PTA₂** (-1.86 V vs Fc^+/Fc) to shift 0.3 V negative of that of **1PTA**. Also observed in the voltammograms is that the reduction of **1PTA₂** is only reversible at scan rates greater than 2 V/s. At scan rates of less than 2 V/s, the return sweep of the voltammograms of **1PTA₂** exhibit two oxidative waves similar to the voltammogram of **1PTA** at the slowest scan rate measured. The decrease in reversibility going from **1** to **1PTA** to **1PTA₂** may be a consequence of the greater electron density on the 2Fe2S core with PTA substitution and/or a consequence of steric factors resulting from the bulky PTA ligands.

Another difference observed between **1** and **1PTA** or **1PTA₂**, is that **1PTA** and **1PTA₂** only undergo initial one-electron reductions, while **1** is known to undergo an initial two-electron reduction. The cathodic peak heights of both **1PTA** and **1PTA₂**, normalized for concentration, were comparable to the peak height of the known one-electron oxidation of ferrocene (data in ESI), while the cathodic peak height corresponding to the two-electron reduction of **1** is double that of ferrocene, **1PTA**, and **1PTA₂**. Previous work on phosphine ligand containing analogues of **1** has concluded that the phosphine ligands have a large effect on the kinetics of a possible second electron transfer.[15] The two-electron reduction of **1** has been attributed to substantial intramolecular rearrangements in the catalyst after the first one-electron reduction. The LUMO of **1** is primarily of Fe-S anti-bond character, and when an electron is added to **1**, an Fe-S bond can cleave along with rotation of the $Fe(CO)_3$ unit and the formation of a bridging CO ligand. The LUMOs of **1PTA** and **$1PTA_2$** are compared to **1** in Fig. 3. All three LUMOs are similar in character, therefore, the orbital character of **1PTA** and **$1PTA_2$** could allow for a two-electron reduction.

The energy of ligand rotation around the Fe centers was then examined computationally to determine if a higher energy rotation of the bulky PTA ligand may prevent the geometric rearrangements necessary for an initial two-electron reduction. In Fig 4 the calculated equilibrium structures of the neutral molecules, **1** and **1PTA,** are compared to calculated rotated transition states that are analogous to the active site of the hydrogenase enzyme.[29] The rotated transition state of **1** consists of a 60^o rotation of one $Fe(CO)_3$ unit, and is calculated to be 38.0 kJ/mol higher in energy than the unrotated equilibrium structure. The rotation of the $Fe(CO)_2PTA$ unit in **1PTA**, also by 60^o, resulted in a higher energy rotation compared to **1**. The rotated transition state of **1PTA** was calculated to be 56.1 kJ/mol higher in energy than the equilibrium structure of **1PTA**.

The activation energy for $Fe(CO)_3$ rotation in **1** is near the low energy end of activation barriers determined for similar complexes.[30-33] Conversely, the calculated energy of rotation for the $Fe(CO)_2PTA$ unit of **1PTA** is larger than other previously reported molecules[32] that have been reported to undergo only one electron reductions at the scan rates used in this study.[34,35] While the rotation of the $Fe(CO)_2PTA$ unit in **1PTA** is calculated as a high energy rotation, **1PTA** still contains an $Fe(CO)_3$ unit that may rotate. However, computations indicate that the high energy rotation of the $Fe(CO)_2PTA$ unit is necessary for the large geometric rotations to occur in **1PTA**. Fig. 5 compares the calculated lowest energy conformation of the completely unrotated **1PTA** anion to two possible conformers of the **1PTA** anion with rotated ligands, which are analogous to $\mathbf{1}^-$ illustrated in Scheme 1. The calculations indicate that the conformation with the rotated $Fe(CO)_2PTA$ unit is 10.4 kJ/mol more stable than the conformer with the $Fe(CO)_3$ unit rotated, but still 6 kJ/mol less stable than the completely unrotated anion of **1PTA**. Conversely, for $\mathbf{1}^-$ the rotated anion was the global minimum energy structure by 2 kJ/mol. Without favored $Fe(CO)_2L$ rotation leading to large geometric reorganizations in the anion of **1PTA**, potential inversion cannot occur and the dianion will not form at the first reduction event observed in the CVs.

Catalytic Activity of 1PTA and 1PTA₂

Both **1PTA** and $\mathbf{1PTA_2}$ exhibit moderate electrocatalytic production of molecular hydrogen in the presence of acetic acid (Fig 6). The peak catalytic current of $\mathbf{1PTA_2}$ is slightly greater than that for **1PTA**, however, the increased catalytic current comes at the cost of increased overpotential. The overpotential associated with the catalytic reduction of acetic acid with $\mathbf{1PTA_2}$ is roughly 0.2 V higher than **1PTA**. This trend of greater catalytic currents being associated with larger overpotentials has been noted previously.[36]

Fig. 6 shows the voltammograms of **1PTA** and $\mathbf{1PTA_2}$ at scan rates of 0.1 V/s. In the absence of acetic acid, both catalysts exhibit initial one electron reductions positive of -2.0 V and no additional reduction peaks more negative than -2.0 V. When acetic acid is added to the solution containing **1PTA**, a new cathodic peak appears near -2.15 V and the peak current increases with increasing concentrations of acetic acid. Similarly, the addition of acetic acid to the solution of **1PTA$_2$** also causes a catalytic peak to appear, but at a potential of -2.35 V. No discernable, consistently linear increase in the initial reduction peak was observed for either catalyst, indicating that the anionic species, **1PTA$^-$** and **1PTA$_2^-$**, are not basic enough to participate in the necessary chemical reactions to catalytically reduce protons from acetic acid at the potential of the first peak. Similar phosphine-containing hydrogenase inspired catalysts have been reported to give a noticeable increase in peak current at the initial reduction potential in the presence of acetic acid.[23,37,38] The lack of an increase in the first reduction peak of **1PTA** and **1PTA$_2$** in the presence of acetic acid further indicates that electron delocalization into the bdt moiety lowers the basicity of the diiron core for this series of catalysts.

To continue the proposed catalytic cycle **1PTA$^-$** and **1PTA$_2^-$** are monoprotonated. The protonated species, **1PTAH** and **1PTA$_2$H**, are then reduced again at the catalytic potentials of -2.15 V and -2.35 V respectively. The reactive anion hydrides, **1PTAH$^-$** and **1PTA$_2$H$^-$**, are able to react with acetic acid in solution and produce molecular hydrogen and regenerate the neutral catalysts to complete the mechanism. While the proposed catalytic mechanisms for **1PTA** and **1PTA$_2$** are similar in some respects to the mechanism of **1**, there are important differences that affect the production of H_2. For the case of the all CO-containing catalyst **1**, the neutral complex acts as a procatalyst and the catalytic cycle only begins when **1$^-$** is produced. The anion, **1$^-$**, then experiences intramolecular rearrangements and is reduced to the dianion at a potential less negative than the initial reduction potential. The formation of the dianion with potential inversion is a critical step, because it opens up a favorable protonation site and creates a dianion that can be readily protonated in the presence of acetic acid. In contrast, the catalytic cycles for **1PTA** and **1PTA$_2$** begin with the neutral species. Neither **1PTA** nor **1PTA$_2$** exhibit potential inversion, therefore, a favorable protonation site similar to **1**$^{2-}$ most likely does not form. The lack of the protonation site, along with not forming a reactive dianion, leads to smaller catalytic peak currents for **1PTA** and **1PTA$_2$** by roughly 100 mA at 50:1 acetic acid to catalyst ratios compared to the parent complex **1**.

Conclusions

Attempts to increase the catalytic activity of **1** by increasing basicity of the 2Fe2S core while maintaining or increasing good solubility characteristics in polar solvents through the substitution of CO ligands with PTA ligands gave varied results. Shifts in the infrared carbonyl stretching frequencies and in the reduction potentials of **1PTA** and **1PTA$_2$** indicated that the addition of PTA ligands to **1** did increase the electron density at the 2Fe2S core. The newly synthesized molecules also successfully catalyzed the reduction of acetic acid to produce H_2. In the absence of a catalyst, the reduction of acetic acid was observed at -2.5 V vs. Fc^+/Fc, while the catalytic reductions were observed at -2.15 V and -2.35 V for **1PTA** and **1PTA$_2$** respectively. These catalytic potentials, however, only exhibited moderate activities at overpotenials near 0.7 to 0.9 V (E^o_{HOAc} = -1.46 V[39]).

While PTA increased the electron density of the 2Fe2S core of the neutral molecules, the bulky ligand may have prevented the formation of a dianionic species similar in geometry to **1**$^{2-}$, which is proposed as an integral aspect of hydrogen production from **1**. High energy rotation of the $Fe(CO)_2PTA$ unit about the Fe center may prevent the necessary intramolecular rearrangements for dianion formation with potential inversion in **1PTA**. Also, the electron-rich **1PTA$_2$** complex forms unstable anions as indicated by the decrease in reversibility observed during reduction in the CVs of **1PTA$_2$**. Thus, to possibly improve the catalysis by **1**, the CO ligands should be substituted with ligands that are only moderate electron donors and are less bulky than PTA.

Acknowledgments. The support of the National Science Foundation through the Collaborative Research in Chemistry program, grant number CHE 0527003, is gratefully acknowledged. The diffractometer was purchased with funding from NSF, grant CHE-0741837.

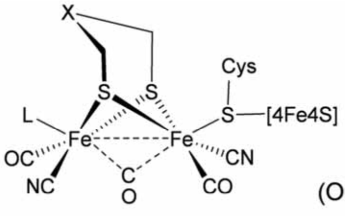

[FeFe] hydrogenase active site

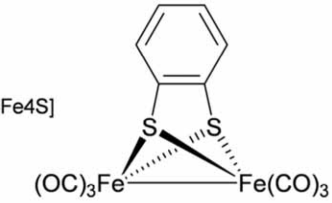

1

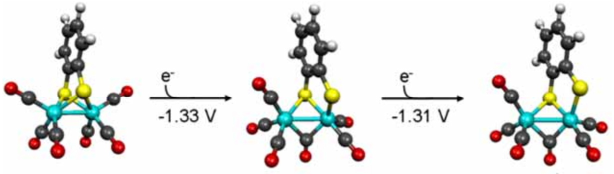

1 **1⁻** **1²⁻**

Scheme 1. Two successive 1e$^-$ reduction of **1** with potential inversion.[7]

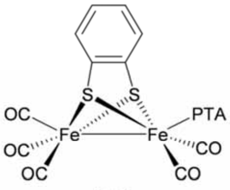

1PTA

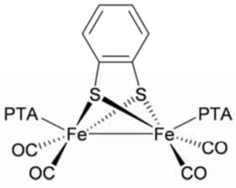

1PTA$_2$

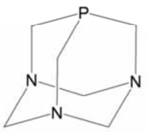

PTA

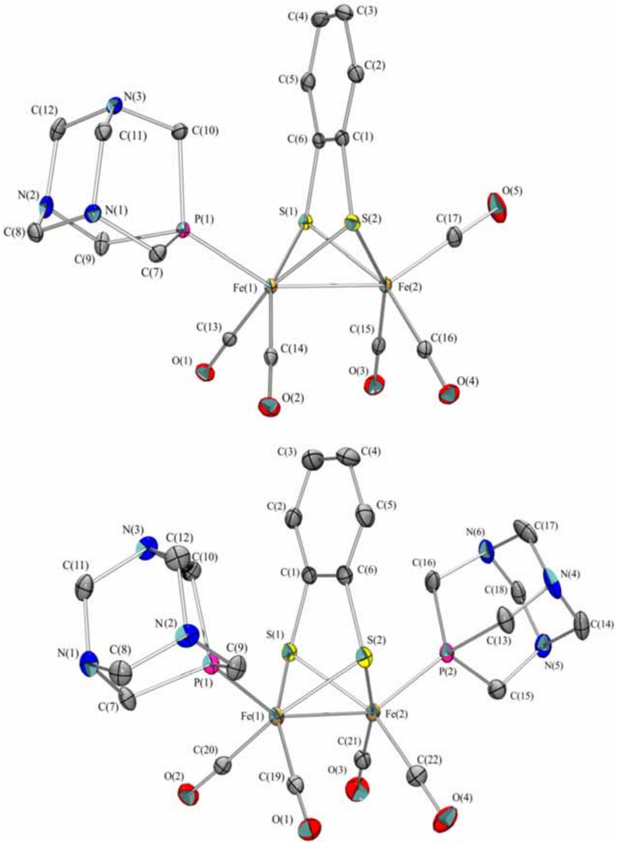

Fig. 1 Structures of **1PTA** (top) and **1PTA$_2$** (bottom, complex A only) obtained by X-ray crystallography. Displacement ellipsoids are at the 30% probability level and hydrogen atoms are omitted.

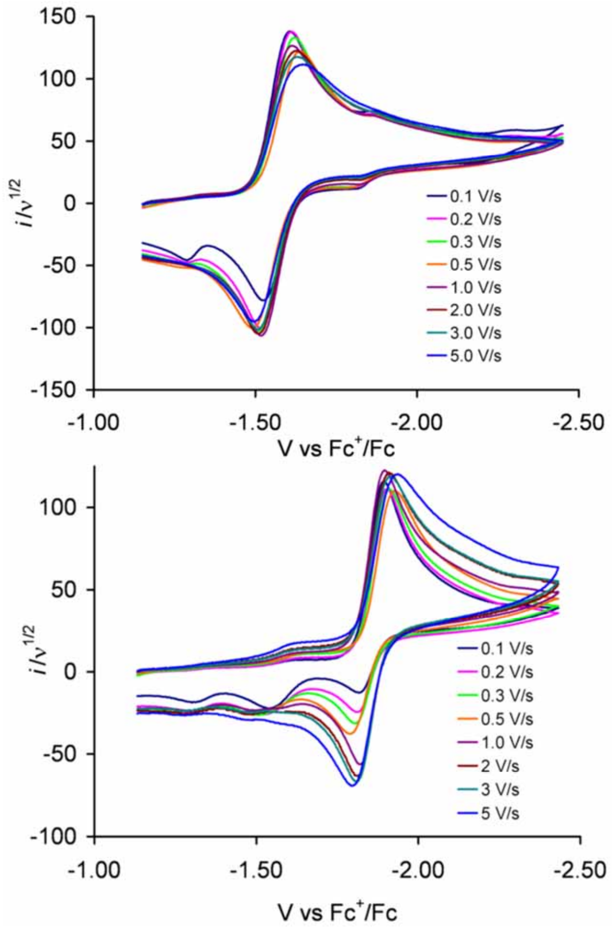

Fig. 2 Effect of scan rate on voltammograms of 1.01 mM **1PTA** (top) and 0.81 mM **1PTA$_2$** (bottom) in acetonitrile under an N_2 atmosphere. ν is the scan rate. Scans were initiated in the negative direstion starting from ca. -1.2 V. $i/\nu^{1/2}$ in units of $\mu As^{1/2}V^{-1/2}$.

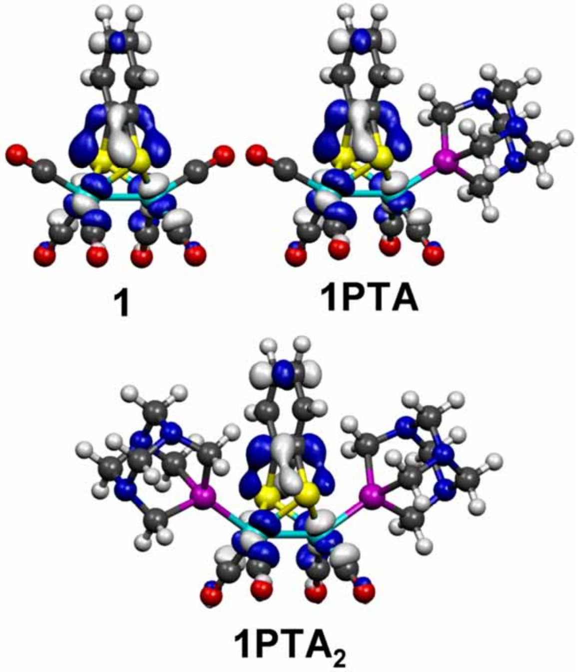

Fig 3. Comparison of the calculated LUMOs of **1**, **1PTA** and **1PTA$_2$**.

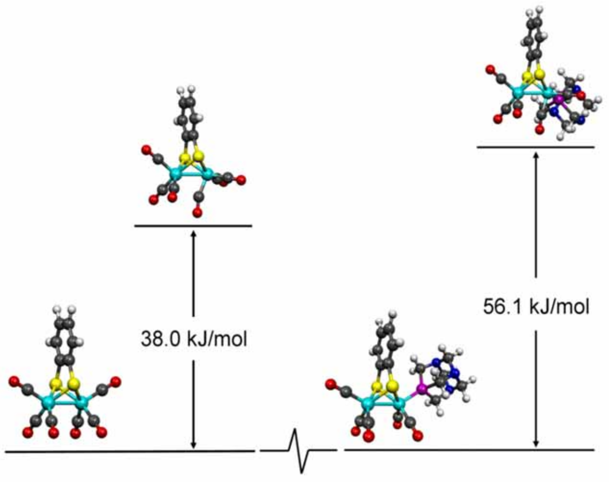

Fig 4. Calculated $Fe(CO)_2L$ (L = PTA, CO) unit rotation energies for **1** (left) and **1PTA** (right) showing the bulky PTA ligand increases the energy required for ligand rotation around the Fe center.

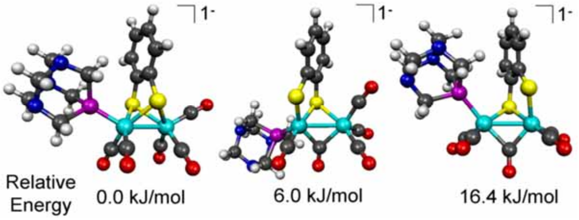

Fig. 5 Two different possible conformations for **1PTA**$^-$ with a Fe(CO)$_2$L (L = CO, PTA) unit rotated, compared to the unrotated anion. Calculations indicate that the unrotated conformation is favored, and the conformation with the Fe(CO)$_2$PTA unit rotated (middle) is the more stable than the conformation with the rotating the Fe(CO)$_3$ unit rotated (right).

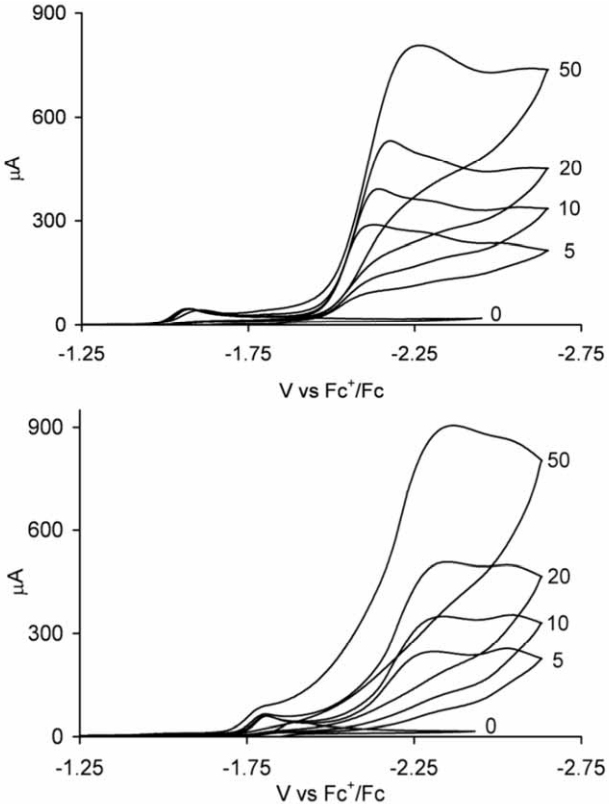

Fig. 6 Voltammograms of 1.01 mM **1PTA** (top) and 0.814 mM **$1PTA_2$** (bottom) in 0.10 M Bu_4NPF_6/CH_3CN at 0.100 V/s in the presence of acetic acid at the concentrations shown in the figure.

Table 1. Experimental crystallographic parameters for **1PTA** and **$1PTA_2$**.

Compound reference	**1PTA**	**$1PTA_2$**
Chemical formula	$C_{17}H_{16}Fe_2N_3O_5PS_2$	$C_{22}H_{28}Fe_2N_6O_4P_2S_2•CH_2Cl_2$
Formula Mass	549.12	763.19
Crystal system	Monoclinic	Monoclinic
a/Å	18.8300(6)	23.1924(10)
b/Å	7.8828(2)	11.8190(5)
c/Å	14.7548(5)	23.2351(10)
α/°	90.00	90.00
β/°	111.827(2)	104.660(2)
γ/°	90.00	90.00
Unit cell volume/Å^3	2033.09(11)	6161.6(5)
Temperature/K	150	150
Space group	$P2_1/c$	$P2_1/n$
Z, Z'	4, 1	8, 2
Reflections measured	39908	120293
Independent reflections	4846	12666
R_{int}	0.0490	0.0676
Final R_1 values ($I > 2\sigma(I)$)	0.0257	0.0402
Final $wR(F^2)$ values ($I > 2\sigma(I)$)	0.0560	0.0981
Final R_1 values (all data)	0.0405	0.0559
Final $wR(F^2)$ values (all data)	0.0615	0.1080
CCDC number[a]	749937	749938

[a] This data can be obtained free of charge from The Cambridge Crystallographic Data Centre via www. ccdc.cam.ac.uk/data_request/cif

Graphical Abstract

Electronic and Geometric Effects by Phosphatriazaadamantane Ligands on the Catalytic Activity of an [FeFe] Hydrogenase Inspired Complex

Aaron K. Vannucci, Shihua Wang, Gary S. Nichol, Dennis L. Lichtenberger, Dennis H. Evans*, and Richard S. Glass**

Contribution from the Department of Chemistry and Biochemistry, The University of Arizona, Tucson, AZ 85721-0041

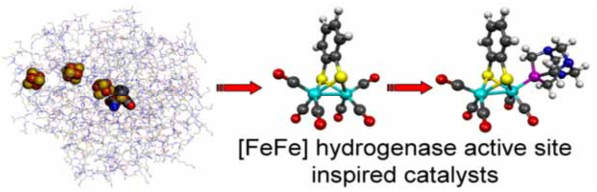

Replacing CO ligands with one or two phosphine ligands in [$Fe_2(\mu\text{-}C_6H_4S_2)(CO)_6$] (**1**) alters the redox chemistry and geometry of **1**, leading to differences in the catalytic production of molecular hydrogen.

References

1 M. Frey, *ChemBioChem,* 2002, **3**, 153-160.

2 G. A. N. Felton, C. A. Mebi, B. J. Petro, A. K. Vannucci, D. H. Evans, R. S. Glass and D. L. Lichtenberger, *J. Organomet. Chem.,* 2009, **694**, 2681-2699.

3 D. M. Heinekey, *J. Organomet. Chem.,* 2009, **694**, 2671-2680.

4 C. Tard and C. J. Pickett, *Chem. Rev.,* 2009, **109**, 2245-2274.

5 J. F. Capon, F. Gloaguen, F. Y. Petillon, P. Schollhammer and J. Talarmin, *Compt. Rend. Chim.,* 2008, **11**, 842-851.

6 J. Capon, F. Gloaguen, F. Y. Pétillon, P. Schollhammer and J. Talarmin, *Coord. Chem. Rev.,* 2009, **253**, 1476-1494.

7 G. A. N. Felton, A. K. Vannucci, J. Chen, L. T. Lockett, N. Okumura, B. J. Petro, U. I. Zakai, D. H. Evans, R. S. Glass and D. L. Lichtenberger, *J. Am. Chem. Soc.,* 2007, **129**, 12521-12530.

8 S. J. Borg, T. Behrsing, S. P. Best, M. Razavet, X. Liu and C. J. Pickett, *J. Am. Chem. Soc.,* 2004, **126**, 16988-16999.

9 A. Darchen, H. Mousser and H. Patin, *Chem. Commun.,* 1988, 968-970.

10 S. P. Best, *Coord. Chem. Rev.,* 2005, **249**, 1536-1554.

11 S. J. Borg, J. W. Tye, M. B. Hall and S. P. Best, *Inorg. Chem.,* 2007, **46**, 384-394.

12 B. E. Bursten, D. J. Darensbourg, G. E. Kellogg and D. L. Lichtenberger, *Inorg. Chem.,* 1984, **23**, 4361-4365.

13 J. Wu, G. M. Bancroft, R. J. Puddephatt, Y. F. Hu, X. Li and K. H. Tan, *Inorg. Chem.,* 1999, **38**, 4688-4695.

14 A. K. Justice, G. Zampella, L. DeGioia, T. B. Rauchfuss, J. I. van der Vlugt and S. R. Wilson, *Inorg. Chem.,* 2007, **46**, 1655-1664.

15 F. Gloaguen, D. Morvan, J. F. Capon, P. Schollhammer and J. Talarmin, *J. Electroanal. Chem.,* 2007, **603**, 15-20.

16 Y. Wang, Z. Li, X. Zeng, X. Wang, C. Zhan, Y. Liu, X. Zeng, Q. Luo and X. Liu, *New J. CHem.,* 2009, **33**, 1780-1789.

17 J. I. van der Vlugt, T. B. Rauchfuss and S. R. Wilson, *Chem. Eur. J.,* 2005, **12**, 90-98.

18 F. Gloaguen, J. D. Lawrence, T. B. Rauchfuss, M. Benard and M. Rohmer, *Inorg. Chem.,* 2002, **41**, 6573-6582.

19 D. Chong, I. P. Georgakaki, R. Mejia-Rodriguez, J. Sanabria-Chinchilla, M. P. Soriaga and M. Y. Darensbourg, *J. Chem. Soc. Dalton Trans.,* 2003, 4158-4163.

20 L. Schwartz, P. S. Singh, L. Eriksson, R. Lomoth and S. Ott, *Comptes Rendus Chimie,* 2008, **11**, 875-889.

21 Z. Wang, J. Liu, C. He, S. Jiang, B. Akermark and L. Sun, *Inorg. Chim. Acta,* 2007, **360**, 2422-2419.

22 Y. Na, M. Wang, K. Jin, R. Zhang and L. Sun, *J. Organomet. Chem.,* 2006, **691**, 5045-5051.

23 R. Mejia-Rodriguez, D. Chong, J. H. Reibenspies, M. P. Soriaga and M. Y. Darensbourg, *J. Am. Chem. Soc.,* 2004, **126**, 12004-12014.

24 J. A. Cabeza, M. A. Martinez-Garcia, V. Riera, D. Ardura and S. Garcia-Granda, *Organometallics,* 1998, **17**, 1471-1477.

25 ADF2006.01d, SCM, Theoretical Chemistry, Vrije Universiteit, Amsterdam,The Netherlands, 2006.

26 G. M. Sheldrick, *SADABS*, 1996.

27 G. M. Sheldrick, *Acta Crystallogr. Sect. A,* 2008, **64**, 112-122.

28 L. J. Farrugia, *J. Appl. Crystallogr.,* 1997, **30**, 565.

29 B. J. Petro, A. K. Vannucci, L. T. Lockett, C. Mebi, R. Kottani, N. E. Gruhn, G. S. Nichol, P. A. J. Goodyer, D. H. Evans, R. S. Glass and D. L. Lichtenberger, *J. Mol. Struct.,* 2008, **890**, 281-288.

30 R. D. Adams, F. A. Cotton, W. R. Cullen, D. L. Hunter and L. Mihichuk, *Inorg. Chem.,* 1975, **14**, 1395-1399.

31 T. C. Flood, F. J. DiSanti and K. D. Campbell, *Inorg. Chem.,* 1978, **6**, 1643-1646.

32 I. P. Georgakaki, L. M. Thomson, E. J. Lyon, M. B. Hall and M. Y. Darensbourg, *Coord. Chem. Rev.,* 2003, **238-239**, 255-266.

33 E. J. Lyon, I. P. Georgakaki, J. H. Reibenspies and M. Y. Darensbourg, *J. Am. Chem. Soc.,* 2001, **123**, 3268-3278.

34 J. Capon, S. Ezzaher, F. Gloaguen, F. Y. Petillon, P. Schollhammer, J. Talarmin, T. J. Davin, J. E. McGrady and K. W. Muir, *New J. Chem.,* 2007, **31**, 2052-2064.

35 G. A. N. Felton, B. J. Petro, R. S. Glass, D. L. Lichtenberger and D. H. Evans, *J. Am. Chem. Soc.,* 2009, **131**, 11290-11291.

36 G. A. N. Felton, A. K. Vannucci, N. Okumura, L. T. Lockett, D. H. Evans, R. S. Glass and D. L. Lichtenberger, *Organometallics,* 2008, **27**, 4671-4679.

37 Z. Wang, J. Liu, C. He, S. Jiang, B. Åkermark and L. Sun, *J. Organomet. Chem.,* 2007, **692**, 5501-5507.

38 P. Li, M. Wang, L. Chen, J. Lui, Z. Zhao and L. Sun, *Dalton Trans.,* 2008, 1919-1926.

39 G. A. N. Felton, R. S. Glass, D. L. Lichtenberger and D. H. Evans, *Inorg. Chem.,* 2007, **46**, 5126-5126.